

A Framework for Holistic KLD-based Waveform Design for Multi-User-Multi-Target ISAC Systems

Yousef Kloob, *Member, IEEE*, Mohammad Al-Jarrah, *Member, IEEE*, and Emad Alsusa, *Senior Member, IEEE*,

Abstract—This paper introduces a novel framework that leverages the Kullback-Leibler Divergence (KLD) metric to analyse and optimise performance trade-offs in integrated sensing and communication (ISAC) systems. We consider a multiple-input multiple-output (MIMO) base station that simultaneously serves communication user equipments (UEs) and detects multiple targets using a shared antenna deployment. We apply this framework to two widely used communication beamforming techniques, maximum ratio transmission (MRT) and zero-forcing (ZF), to assess their impact on the radar subsystem’s performance. Additionally, two optimisation problems are formulated: the first optimises the radar subsystem’s KLD under communication constraints, and the second focuses on communication waveform KLD optimisation with constraints on the radar KLD. These problems are solved using a projected gradient method with adaptive penalties for the radar waveforms and a gradient-assisted interior point method (IPM) for the communication waveforms. Through theoretical derivations and extensive simulations, we demonstrate that our KLD approach effectively characterises and optimises the performance trade-offs between sensing and communication in ISAC systems. The results show significant improvements in both radar detection and communication performance when compared to traditional MRT and ZF beamforming, and the identity covariance design for radar subsystems. These findings promote a more holistic design and optimisation of ISAC for next-generation wireless networks and demonstrate the advantages of KLD-based optimisation in balancing the performance of both sensing and communication.

Index Terms—Integrated sensing and communication, multiple-input-multiple-output (MIMO), radar, zero-forcing, maximum ratio transmission, beamforming, optimisation, Kullback–Leibler divergence (KLD).

I. INTRODUCTION

THE rapid evolution of wireless communication networks has dramatically expanded the landscape of interconnected devices to include new applications such as autonomous vehicles and unmanned aerial vehicles (UAVs) that are heavily dependent on advanced sensing, pushing the boundaries of communication systems beyond their traditional limits [1]–[4]. As we approach the sixth-generation (6G) era, network operators and service providers aim not only to further enhance their communication services but also to include advanced sensing-based applications such as detection, localisation, tracking, navigation, and environmental surveillance [5]–[7].

Integrated Sensing and Communications (ISAC) systems have gained significant interest as a key enabler of many 6G applications. ISAC aims to synergistically merge sensing and communication functionalities hence optimising base station (BS) resources for dual purposes [8]–[13]. This integration can be achieved through various approaches. For example, in a

separated deployment, the BS antennas are allocated distinctly between communication and radar subsystems, which can simplify the system design but may underutilise resources. In contrast, the shared deployment strategy employs all antennas for both functionalities, hence offering higher resource efficiency, but at the cost of increased complexity due to the need for more sophisticated signal processing techniques [14], [15].

The evolution of ISAC has been accelerated by advances in multi-antenna technologies, particularly massive Multiple-Input Multiple-Output (MIMO) systems. These systems allow for the generation of highly directional beams and support simultaneous services to a large number of users, thereby significantly enhancing both communication capacity and sensing accuracy [16]. The synergy between ISAC and massive MIMO presents a promising avenue for meeting the stringent requirements of future wireless networks. However, evaluating the performance of ISAC systems poses unique challenges due to their dual functionality. Traditionally, communication and sensing subsystems have been assessed using distinct metrics, with communication performance measured by achievable rate, outage probability, and bit error rate (BER), while the sensing performance is typically evaluated using metrics like estimation rate, detection probability, false alarm probability, and mean square error (MSE) [17]. This disparity complicates the holistic assessment and optimisation of ISAC systems.

A. Literature review

To address these challenges mentioned above, there has been a growing interest in developing unified performance measures that can simultaneously capture both sensing and communication capabilities. One such measure that has gained traction is the Kullback-Leibler divergence (KLD), also known as the relative entropy. KLD has a well-established history in information theory and has been extensively used in the analysis and design of sensing systems, particularly in the context of MIMO radars [18]–[20]. It quantifies the dissimilarity between two probability distributions, serving as a measure of the information gain achieved by using one distribution over another. While the application of KLD in sensing systems is well-established, its potential in characterising communication system performance remains open. Recent studies have begun to bridge this gap, demonstrating the utility of KLD in assessing the performance trade-offs between sensing and communication functionalities in ISAC systems. For instance, in our previous works [21], [22], we employed KLD to analyse performance in systems with separated antenna deployment, while in [23] we proposed a low-complexity unified objective function based on KLD, aimed at optimising network resources for both separated and shared deployment scenarios. Moreover, further insights about the achievable

Y. Kloob, M. Al-Jarrah and E. Alsusa are with the Department of Electrical and Electronic Engineering, University of Manchester, Manchester M13 9PL, U.K. (e-mail: {yousef.kloob, mohammad.al-jarrah, e.alsusa}@manchester.ac.uk).

KLD trade-off in ISAC systems are explored in [24], and more designs have been discovered. Nonetheless, the literature lacks a comprehensive investigation and beamforming design for a generalised multi-user-multi-target (MUMT) ISAC system using the promising KLD.

Further efforts have explored various optimisation approaches for ISAC systems, each addressing specific aspects of system performance. For example, joint radar-communication beamforming optimisation based on the Cramér-Rao Bound (CRB) has been proposed to improve both sensing and communication performance [25]. This approach minimises the CRB of angle estimation for radar while maximising the signal-to-interference-plus-noise ratio (SINR) for communication, thus enhancing the accuracy of sensing and the quality of communication simultaneously. However, these methods often focus on optimising individual components rather than adopting a unified framework that captures the interplay between different functionalities. Beamforming optimisation has been a particular focus, with studies investigating partially connected hybrid beamforming designs to address the hardware complexity of fully digital systems [26]. While these approaches offer practical advantages in terms of implementation, they do not fully capture the nuanced trade-offs between sensing and communication performance, especially in deeply integrated scenarios. Waveform optimisation has also been extensively studied, with recent work proposing a symbol-level precoding scheme using a faster-than-Nyquist approach to enhance the spectral efficiency in bandwidth-constrained environments [27]. This approach focuses on communication waveform design while considering the radar functionality as a constraint, ensuring that the designed waveforms maintain certain radar performance metrics. However, this work does not consider a unified optimisation framework that could simultaneously address the needs of both subsystems.

B. Motivation and contribution

Despite these advances, current approaches often fall short of fully exploiting the potential of integrated systems. Most notably, there is a need for more comprehensive models that can accurately reflect the real-world operation of ISAC systems, particularly in scenarios where communication signals can be utilised for radar target detection alongside dedicated radar signals. Exploiting the interference from communication signals as a source of information for radar operations enhances radar detection capabilities, improving the system's overall resource efficiency [14]. This dual-use of communication signals represents a significant departure from traditional approaches, which typically treat interference as a detrimental factor to be mitigated rather than leveraged [28], [29].

Toward these objectives and motivated by the fact that KLD is able to provide a unified measure for ISAC system holistically, this paper proposes a novel framework based on the Kullback-Leibler divergence (KLD) to characterise and optimise the sensing-communication performance trade-offs in shared antenna deployment ISAC systems. This work addresses several gaps in the existing literature by introducing a unified KLD-based performance measure that captures the synergies and trade-offs between sensing and communication

in ISAC systems. By considering the shared deployment scenario and proposing specific optimisation techniques for both subsystem waveforms, we provide a comprehensive approach for system optimisation that reflects the true potential of ISAC systems in future wireless networks. Additionally, our analysis of different beamforming techniques within this framework offers valuable guidance for designing ISAC systems to effectively balance the needs of both subsystem functionalities. Our system model consists of a multiple-input-multiple-output (MIMO) base station (BS) that simultaneously serves communication user equipment (UEs) and detects multiple targets using shared resources. The key contributions of this work are:

- **Unified Performance Measure:** We derive the Kullback-Leibler Divergence (KLD) specifically for the integrated operation of communication and radar systems within ISAC. This performance measure unifies the communication error rate with radar target detection capabilities into a single objective function. By deriving this KLD-based metric for communication and radar components, we optimise ISAC system design holistically, addressing the trade-offs and enhancing overall system performance.
- **Exploitation of Communication Interference:** Our framework accounts for the fact that communication signals can also be exploited for radar target detection alongside dedicated radar signals, providing a more comprehensive and useful model of ISAC system operation. This dual-use approach enhances the radar performance by utilising communication interference as an additional source of information for target detection.
- **KLD-based Optimised ISAC:** We propose two novel optimisation techniques: radar and communication waveform KLD-based optimisation. Both maximise their respective KLD measures subject to the minimum KLD of both subsystems and power constraints. The non-convex radar optimisation employs a projected gradient method with an adaptive penalty, while the communication optimisation uses a gradient-assisted interior point method. These techniques efficiently handle ISAC waveform design's complex, multi-dimensional nature, enabling balanced performance optimisation across both subsystems within system constraints.
- **Benchmark Analysis:** We investigate two benchmark beamforming techniques for the communication subsystem, namely maximum ratio transmission (MRT) and zero-forcing (ZF), and analyse their impact on the overall system performance within our KLD-based framework. This analysis provides practical insights for optimising ISAC performance in shared deployment scenarios, considering the complexity-performance trade-off.

Our results demonstrate that the proposed KLD-based optimisation techniques significantly enhance ISAC system performance compared to the MRT and ZF scenarios for the communication subsystem and the radar subsystem's conventional identity covariance design. The radar waveform optimisation shows substantial improvements in both target detection and communication performance, while the communication waveform optimisation primarily benefits the communication sub-

system with modest radar performance gains. Both techniques exhibit robust performance across varying SNR levels, with the radar optimisation demonstrating particularly stable computational efficiency. Notably, incorporating communication signals in radar detection significantly enhances overall system performance, especially in scenarios with limited dedicated radar resources. These findings provide valuable insights for designing efficient shared deployment ISAC systems that balance sensing and communication requirements.

C. Paper organisation

The paper is structured as follows. Section II presents the system model. Sections III and IV analyse the communication and radar systems, respectively, including the derivations of KLD for each system. In Section V, the first KLD-based optimisation technique considers the radar KLD sum under communication KLD constraint is investigated. Section VI introduces the second KLD-based optimisation technique based on communication KLD sum with radar KLD constraint. Section VII displays the numerical results, and finally, Section VIII concludes the work.

Notation: Bold uppercase letters (e.g., \mathbf{S}) denote matrices, and bold lowercase letters (e.g., \mathbf{s}) denote vectors. Superscripts $(\cdot)^*$, $(\cdot)^T$, and $(\cdot)^H$, denote the conjugate, transpose, and Hermitian transpose, respectively. Subscripts $(\cdot)_c$ and $(\cdot)_r$ relate to the communication, and radar subsystems, respectively.

II. SYSTEM MODEL

We consider an N antenna MIMO-BS. The antennas are utilised for detecting a maximum number of T targets and serving K number of single-antenna communication UEs in the downlink direction in shared deployment manner. The total transmitted power available at BS is P_T which is utilised for both sensing and data communication duties. The power P_T allocated to the radar and communication subsystems are denoted as P_r and P_c , where $P_T = P_c + P_r$. As a starting point, non-optimised beamforming techniques such as MRT and ZF are employed at BS to precode the information of communication UEs [16]. These techniques serve as benchmarks for our subsequent optimised systems, which will be introduced and analysed later in Sections V and VI. The combined transmitted ISAC signal $\mathbf{x}_l \in \mathbb{C}^{N \times 1}$ will be as follows,

$$\mathbf{x}_l = \mathbf{W}_c \mathbf{s}_{c,l} + \mathbf{W}_r \mathbf{s}_r, \quad (1)$$

where $\mathbf{s}_{c,l} \in \mathbb{C}^{K \times 1}$ is a vector of communication UEs symbols, $\mathbf{s}_r \in \mathbb{C}^{T \times 1}$ is a vector of the baseband radar waveforms for the potential targets, $\mathbf{W}_c \in \mathbb{C}^{N \times K}$ represents the precoding matrix for the communication subsystem, and $\mathbf{W}_r \in \mathbb{C}^{N \times T}$ represents the precoding matrix for the radar subsystem. The transmitted signals vector \mathbf{x}_l is transmitted from the BS and received at the UEs as well as the targets which reflect the received \mathbf{x}_l back to the BS. Although the radar signal component received at the UEs might cause interference that cannot be eliminated by the users, the communication signal component received at the targets and reflected back to the BS carries information about the target. Therefore, by carefully designing the precoding matrices at the BS, the sensing information can be enhanced by exploiting the

communication signal. This dual-use approach enhances the radar performance by utilising the communication signal as an additional source of information. The radar waveform design is based on the combined transmit signal covariance matrix for the t -th beam where the covariance matrix of the t -th transmit beam is $\mathbf{R}_t = \frac{1}{L} \sum_{l=1}^L \mathbf{x}_{t,l} \mathbf{x}_{t,l}^H$, $\mathbf{x}_{t,l} = \mathbf{w}_{r,t,l} \mathbf{s}_r + \mathbf{W}_c \mathbf{s}_{c,l}$, and L is the total number of snapshots. This formulation allows us to incorporate the communication signals into the radar detection process. It should be noticed that the power for the radar is integrated into the precoding vector $\mathbf{w}_{r,t,l}$, where it is designed to have $\|\mathbf{w}_{r,t,l}\|_F^2 = \frac{P_r}{T}$, and $\mathbf{w}_{r,t,l} = \frac{P_r}{NT} \tilde{\mathbf{w}}_{r,t,l}$, where $\tilde{\mathbf{w}}_{r,t,l}$ is the t th beam precoding vector, and $\|\cdot\|_F$ is the Frobenius norm.

A. Communication System

At each l instance, a data symbol $s_{c,k,l}$ intended for the k -th UE is drawn from a normalised constellation, i.e. $\mathbb{E}[|s_{c,k,l}|^2] = 1$. The received signal at the k -th UE can be formulated as

$$y_{c,k,l} = \underbrace{\mathbf{h}_k^T d_{c,k}^{-\zeta/2} \mathbf{w}_{c,k} s_{c,k,l}}_{\text{Desired } k\text{-th UE signal}} + \underbrace{\omega_{MN,k}}_{\text{Inter-user interference}} + \underbrace{\eta_k}_{\text{Radar interference and noise}}, \quad (2)$$

where $\mathbf{h}_k \in \mathbb{C}^{N \times 1} \sim \mathcal{CN}(0, \sigma_h^2)$ represents the channel from the BS to the k -th UE, $\omega_{MN,k} = \sum_{i=1, i \neq k}^K \mathbf{h}_k^T d_{c,k}^{-\zeta/2} \mathbf{w}_{c,i} s_{c,i,l}$ represents the IUI on the k -th UE from the other UEs, $d_{c,k}^{-\zeta/2}$ is the channel pathloss from BS to the k -th UE with $d_{c,k}$ representing the distance from BS to the k -th UE, and ζ is the pathloss exponent $\eta_k = \mathbf{h}_k^T d_{c,k}^{-\zeta/2} \mathbf{W}_r \mathbf{s}_r + n_{k,l}$ is the interference-plus-noise term with $n_{k,l} \sim \mathcal{CN}(0, \sigma_n^2)$ representing the additive white Gaussian noise (AWGN). The precoding vector for the communication system is $\mathbf{w}_{c,k} \in \mathbb{C}^{N \times 1}$, which is typically designed based on the given channel matrix from MIMO-BS to UEs $\mathbf{H} \in \mathbb{C}^{N \times K} = [\mathbf{h}_1, \dots, \mathbf{h}_k, \dots, \mathbf{h}_K]$, where the elements of \mathbf{H} are independent and identically distributed (i.i.d) complex Gaussian random variables with zero mean and variance σ_h^2 . In the next two subsections, we revisit the conventional MRT and ZF designs which are typically used to precode the communication data symbols at the BS. These precoding schemes will serve as benchmarks for our designs.

1) *MRT beamforming:* In MRT precoding, the amount of received power at the UEs is maximised without taking into account the imposed interference. This approach usually leads to acceptable performance at low SNR values but its performance deteriorates at large SNRs. The normalised MRT beamforming matrix is designed for all UEs based on the channel matrix as follows,

$$\mathbf{W}_c = \mathbf{P} \mathbf{H}^* / \|\mathbf{H}\|_F = \mathbf{P} [\mathbf{h}_1^*, \dots, \mathbf{h}_K^*] / \|\mathbf{H}\|_F, \quad (3)$$

where $\mathbf{P} \in \mathbb{C}^{K \times K} = \text{diag}(\sqrt{p_1}, \dots, \sqrt{p_K})$ is the power allocation matrix for the communication users, which is a diagonal matrix that controls the power allocated for each UE.

2) *ZF beamforming:* On the contrary, ZF precoding eliminates inter-user interference (IUI) at the UEs regardless of the amount of the received power. This approach usually results in excellent performance at high SNR values. The normalised ZF beamforming matrix is designed also based on the channel matrix, and can be represented as follows,

$$\mathbf{W}_c = \mathbf{P}\tilde{\mathbf{W}}_c / \|\tilde{\mathbf{W}}_c\|_F \quad (4)$$

where $\tilde{\mathbf{W}}_c = \mathbf{H}^H (\mathbf{H}\mathbf{H}^H)^{-1}$ is the ZF beamformer before normalisation.

B. Radar system

The radar system is designed for high adaptability, allowing for real-time adjustments in detection capabilities across L frame snapshots. T represents the radar beams emitted during a specific detection frame. Using MIMO radar technology, multiple beams can be generated simultaneously using orthogonal signals [30], [31], where T signifies the upper limit of detectable targets in a single frame.

The system explores multiple angular-range-Doppler bins over successive frames, increasing target identification. Its flexibility in varying emitted beams allows for the simultaneous detection of more targets, to fine-tune the system's detection capability according to different operational demands. However, it is crucial to acknowledge that the value of T is constrained by the available antennas and UEs serviced by the BS, highlighting the need for efficient waveform design and resource allocation in ISAC systems.

Our focus aligns with scenarios where targets are spatially separated, with each target confined to a distinct radar bin, as per prior studies [32], [33]. The literature presents algorithms to separate signals from closely spaced or unresolved targets, facilitating accurate target enumeration [34]. The total radar return signal at the l -th snapshot is shown as follows,

$$\mathbf{y}_{r,l} = \sum_{t=1}^T \mathbf{H}_t^T d_{r,t}^{\zeta/2} \mathbf{w}_{r,t,l} s_{r,t} + \mathbf{H}_t^T d_{r,t}^{\zeta/2} \mathbf{W}_c \mathbf{s}_{c,l} + \mathbf{n}_l, \quad (5)$$

where $\mathbf{H}_t \in \mathbb{C}^{N \times N}$ is the target response matrix of the BS-Target-BS route for the t -th target, following a Rayleigh distribution [35]. The $\mathbf{n}_l \sim \mathcal{CN}(\mathbf{0}, \sigma_n^2 \mathbf{I}_N)$ is the additive white Gaussian noise vector at the l -th snapshot. To analyse the radar returns from all beams, a series of matched filters are typically applied, each tuned to a specific waveform $s_{r,t} : \forall t = \{1, 2, \dots, T\}$, which corresponds to a particular radar angular-range-Doppler bin. Because $s_{r,t}$ is orthogonal to $s_{r,i}$ for all $t \neq i$, the radar returns from distinct beams can be effectively separated, enabling independent detection of each potential target. The radar precoding matrix $\mathbf{W}_{r,l}$ is designed such that the covariance matrix is $\mathbf{R}_w \triangleq \frac{1}{L} \sum_{l=1}^L \mathbf{W}_{r,l} \mathbf{W}_{r,l}^H \in \mathbb{C}^{N \times N}$. The received signal for the t -th target at the BS, under the binary hypotheses $\mathcal{H}_q \forall q \in \{0, 1\}$, where \mathcal{H}_1 signifies target presence and \mathcal{H}_0 denotes target absence, can be mathematically represented as follows,

$$\mathbf{y}_{r,t,l|\mathcal{H}_q} = \mathbf{H}_t^T d_{r,t}^{\zeta/2} \mathbf{w}_{r,t,l} q + \mathbf{H}_t^T d_{r,t}^{\zeta/2} \mathbf{W}_c \mathbf{s}_{c,l} q + \mathbf{n}_{t,l}, \quad (6)$$

The $\mathbf{n}_{t,l} \sim \mathcal{CN}(\mathbf{0}, \sigma_n^2 \mathbf{I}_N)$ is the additive white Gaussian noise vector at the l -th snapshot.

III. THE COMMUNICATION KLD: ZF AND MRT

In this section, we derive the KLD of the communication system for the MRT and ZF beamforming using the shared deployment antenna configuration. The analysis is carried out for the normalised precoders introduced in Section II-A.

To derive the KLD, it is necessary to establish the statistical properties of the signal, IUI, radar interference, and noise. For a pair of multivariate Gaussian distributed random variables having mean vectors of μ_m and μ_n and covariance matrices of Σ_m and Σ_n , the KLD can be derived as,

$$\text{KLD}_{n \rightarrow m} = \frac{1}{2 \ln 2} \left(\text{tr}(\Sigma_n^{-1} \Sigma_m) - 2 + (\mu_n - \mu_m)^T \times \Sigma_n^{-1} (\mu_n - \mu_m) + \ln \frac{|\Sigma_n|}{|\Sigma_m|} \right). \quad (7)$$

A. MRT beamforming

For the MRT precoding scheme, the analysis encompasses the desired signal, IUI, radar interference, and noise components. The examination starts with the IUI term, which is the second term in (2), given by,

$$\omega_{\text{MN},k} = d_{c,k}^{-\zeta/2} \mathbf{h}_k^T \sum_{\substack{i=1 \\ i \neq k}}^K \mathbf{w}_{c,i} s_{c,i,l} = \frac{d_{c,k}^{-\zeta/2}}{\|\mathbf{H}\|_F} \sum_{\substack{i=1 \\ i \neq k}}^K \mathbf{h}_k^T \mathbf{h}_i^* \sqrt{p_i} s_{c,i,l}. \quad (8)$$

Since the elements of \mathbf{h}_k and $\mathbf{h}_i \forall i \neq k$ are i.i.d. complex Gaussian random variables with zero mean and variance σ_h^2 , the term $\mathbf{h}_k^T \mathbf{h}_i^*$ is the inner product of two independent complex Gaussian vectors. Thus, the central limit theorem (CLT) can be invoked to show that the distribution of $\mathbf{h}_k^T \mathbf{h}_i^*$ tends to be complex Gaussian with zero mean and variance $N\sigma_h^4$ for a large number of antennas N . Meanwhile, the normalisation term $\|\mathbf{H}\|_F^2 = \sum_{i=1}^K \|\mathbf{h}_i\|^2$ follows a chi-squared distribution with $2NK$ degrees of freedom, scaled by $\sigma_h^2/2$. Consequently, the exact distribution of $\omega_{\text{MN},k}$ is a ratio of complex normal variables to the square root of a chi-squared variable. This ratio distribution does not have a simple closed-form expression. However, we can approximate its behaviour for large N and K , by using the law of large numbers, $\|\mathbf{H}\|_F^2 \approx NK\sigma_h^2$. Using this approximation, we can write (8) as,

$$\omega_{\text{MN},k} \approx \frac{d_{c,k}^{-\zeta/2}}{\sqrt{NK\sigma_h^2}} \sum_{\substack{i=1 \\ i \neq k}}^K \mathbf{h}_k^T \mathbf{h}_i^* \sqrt{p_i} s_{c,i,l}. \quad (9)$$

ω_{MN} is a sum of independent complex normal variables. By invoking CLT, for large KN , the sum approaches a complex normal distribution with zero mean and a variance of

$$\sigma_{\omega, \text{MN}}^2 \approx \frac{d_{c,k}^{-\zeta}}{NK\sigma_h^2} \sum_{i \neq k} N\sigma_h^4 p_i = \frac{d_{c,k}^{-\zeta} \sigma_h^2}{K} \sum_{i \neq k} p_i, \quad (10)$$

The accuracy of the approximated density of ω_{MN} is validated by simulation, which compares it with simulated density functions under different values of N . It can also be shown that the distribution of η_k is well approximated by a complex Gaussian distribution using CLT, particularly for large N . This approximation yields a mean of $\mathbb{E}[\eta_k] = 0$, and a variance of

$$\sigma_{\eta}^2 = d_{c,k}^{-\zeta} \mathbb{E}[\|\mathbf{h}_k^T \mathbf{W}_{r,l}\|^2] + \sigma_n^2 = d_{c,k}^{-\zeta} P_r \sigma_h^2 + \sigma_n^2 \quad (11)$$

where $\mathbf{R}_{w,t} = \frac{1}{L} \sum_{l=1}^L \tilde{\mathbf{w}}_{r,t,l} \tilde{\mathbf{w}}_{r,t,l}^H$. Now, the equivalent IUI and radar interference plus noise term $\tilde{\omega}_{\text{MN},k} = \omega_{\text{MN}} + \eta_k$ can be approximated as a complex Gaussian random variable

with zero mean and variance $\sigma_{\omega, \text{MN}}^2 + \sigma_{\eta}^2$. In order to find the KLD for the MRT case with matrix normalisation, we need to evaluate the expected value of the desired signal power, which is represented by the first term in (2). This term, $|\mathbf{h}_k^T \mathbf{w}_{c,k}|^2$ can be expressed as follows,

$$|\mathbf{h}_k^T \mathbf{w}_{c,k}|^2 = |\mathbf{h}_k^T \mathbf{h}_k^*|^2 / \|\mathbf{H}\|_F^2 = \|\mathbf{h}_k\|^4 / \|\mathbf{H}\|_F^2. \quad (12)$$

The expected value of this term can be approximated using the properties of the chi-squared distribution and the approximation $\mathbb{E}[1/X] \approx 1/\mathbb{E}[X]$ for a random variable X ,

$$\mathbb{E}[|\mathbf{h}_k^T \mathbf{w}_{c,k}|^2] \approx p_k \mathbb{E}[\|\mathbf{h}_k\|^4] / \mathbb{E}[\|\mathbf{H}\|_F^2] = p_k(N+1)\sigma_h^2/K. \quad (13)$$

Given that $\Sigma_n = \Sigma_m = (\sigma_{\omega, \text{MN}}^2 + \sigma_{\eta}^2)\mathbf{I}_2$, and $\mu_{k,m} = d_{c,k}^{-\zeta/2} \mathbb{E}[\mathbf{h}_k^T \mathbf{w}_{c,k}] s_{c,k,l}^{(m)}$, and $\mu_{k,n} = d_{c,k}^{-\zeta/2} \mathbb{E}[\mathbf{h}_k^T \mathbf{w}_{c,k}] s_{c,k,l}^{(n)}$, substituting these into equation (7), then the KLD can be found as [21, Corollary 1],

$$\text{KLD}_{c,k}^{\text{MRT}} = \frac{\lambda d_{c,k}^{-\zeta} \mathbb{E}[|\mathbf{h}_k^T \mathbf{w}_{c,k}|^2]}{(\sigma_{\omega, \text{MN}}^2 + \sigma_{\eta}^2)M(M-1) \ln 2}, \quad (14)$$

where $\lambda = \sum_{m=1}^M \sum_{\substack{n=1 \\ n \neq m}}^M |s_{c,k,l}^{(n)} - s_{c,k,l}^{(m)}|^2$ is constant for a given constellation, for example, for MPSK signalling, $\lambda_{\text{MPSK}} = 2 \sum_{m=1}^M \sum_{\substack{n=1 \\ n \neq m}}^M (1 - \cos(\phi_{k,m} - \phi_{k,n}))$. Substituting (13) in (14), the KLD for MRT precoding with matrix normalisation is,

$$\text{KLD}_{c,k}^{\text{MRT}} = \frac{\lambda d_{c,k}^{-\zeta} p_k(N+1)\sigma_h^2}{K(\sigma_{\omega, \text{MN}}^2 + \sigma_{\eta}^2)M(M-1) \ln 2}. \quad (15)$$

B. ZF beamforming

With ZF precoding, the received signal at the k -th user is,

$$y_{k,l} = \mathbf{h}_k^T d_{c,k}^{-\zeta/2} \mathbf{w}_{c,k} s_{c,k,l} + \mathbf{h}_k^T d_{c,k}^{-\zeta/2} \mathbf{W}_{r,l} \mathbf{s}_r + n_{k,l}, \quad (16)$$

where $\mathbf{w}_{c,k}$ is the k -th column of the normalised ZF precoding matrix. Note, that the term $\sum_{i=1, i \neq k}^K \mathbf{h}_k^T d_{c,k}^{-\zeta/2} \mathbf{w}_{c,i} s_{c,i,l} = 0$ as the ZF precoder eliminates the IUI. The mean vectors and covariance matrices for the n -th and m -th symbols are given by,

$$\begin{aligned} \boldsymbol{\mu}_{k,j} &= d_{c,k}^{-\zeta/2} \mathbb{E}[\mathbf{h}_k^T \mathbf{w}_{c,k}] s_{c,k,l}^{(j)} \\ &= d_{c,k}^{-\zeta/2} \mathbb{E}[\|\tilde{\mathbf{W}}_c\|_F^{-2}] s_{c,k,l}^{(j)}, \quad j \in \{n, m\}, \end{aligned} \quad (17)$$

$$\Sigma_n = \Sigma_m = \sigma_{\eta}^2, \quad (18)$$

where $\mathbb{E}[\mathbf{h}_k^T \mathbf{w}_{c,k}] = 1$ due to the normalisation of the ZF precoding matrix. Since $\|\tilde{\mathbf{W}}_c\|_F^{-2} = \text{tr}((\mathbf{H}\mathbf{H}^H)^{-1})$, under flat fading channel, $\|\tilde{\mathbf{W}}_c\|_F^{-2}$ follows a Gamma distribution with shape parameter $N - K + 1$ and scale parameter 1, denoted as $\|\tilde{\mathbf{W}}_c\|_F^{-2} \sim \text{Gamma}(L_G, 1)$, where $L_G = N - K + 1$. Let $x \triangleq \|\tilde{\mathbf{W}}_c\|_F^{-2}$. By substituting (17), and (18) in (7), then the KLD becomes,

$$\text{KLD}_{c,k}^{\text{ZF}} = \frac{\lambda d_{c,k}^{-\zeta} p_k}{M(M-1)\sigma_{\eta}^2 \ln 2} \mathbb{E} \left[\frac{1}{\|\tilde{\mathbf{W}}_c\|_F^2} \right], \quad (19)$$

The expectation of $1/\|\tilde{\mathbf{W}}_c\|_F^2$ can be calculated using the PDF of Gamma distribution as follows,

$$\mathbb{E} \left[\|\tilde{\mathbf{W}}_c\|_F^{-2} \right] = \int_0^{\infty} \frac{1}{x} \cdot \frac{1}{\Gamma(L_G)} x^{L_G-1} e^{-x} dx = N - K. \quad (20)$$

Substituting this result into (19), we get the final KLD $_{c,k}^{\text{ZF}}$,

$$\text{KLD}_{c,k}^{\text{ZF}} = \lambda d_{c,k}^{-\zeta} p_k(N-K)/M(M-1)\sigma_{\eta}^2 \ln 2. \quad (21)$$

C. Conditional KLD for an Arbitrary Precoding Matrix \mathbf{W}_c and Given Channel Matrix

A conditional KLD for communication, in terms of the beamforming matrix \mathbf{W}_c and for a given channel matrix \mathbf{H} , is required to formulate an optimisation problem. Considering the received signal representation in (2), the conditional mean vectors and variance are,

$$\mu_{k,j} = \mathbb{E}[y_{c,k,l}^{(j)}] = \mathbf{h}_k^T d_{c,k}^{-\zeta/2} \mathbf{w}_{c,k} s_{c,k,l}^{(j)}, \quad j \in \{n, m\}, \quad (22)$$

$$\begin{aligned} \text{Var}(y_{c,k,l}^{(j)}) &= \mathbb{E}[|y_{c,k,l}^{(j)} - \mu_{k,n}|^2] \\ &= d_{c,k}^{-\zeta} \sum_{i=1, i \neq k}^K \|\mathbf{h}_k^T \mathbf{w}_{c,i}\|^2 + \sigma_{\eta}^2, \quad j \in \{n, m\}, \end{aligned} \quad (23)$$

Note that, the variance of the received signal for a given pair of symbols $\{s_{c,k,l}^{(n)}, s_{c,k,l}^{(m)}\} \forall \{m, n\}, m \neq n$ is equal. Thus, the covariance is,

$$\Sigma_{c,n} = \Sigma_{c,m} = d_{c,k}^{-\zeta} \sum_{i=1, i \neq k}^K \|\mathbf{h}_k^T \mathbf{w}_{c,i}\|^2 + \sigma_{\eta}^2 \quad (24)$$

Substituting the mean vectors and covariance matrices from (22), and (24) into the KLD expression given in (7), we can obtain the KLD for the k -th UE in the communication subsystem for each possible pair of unequal data symbols $\{s_{c,k,l}^{(n)}, s_{c,k,l}^{(m)}\}, n \neq m$, this is done as follows,

$$\begin{aligned} \text{KLD}_{k,m \rightarrow n} &= \frac{d_{c,k}^{-\zeta}}{2 \ln 2} \left(\left(\mathbf{h}_k^T \mathbf{w}_{c,k} (s_{c,k,l}^{(m)} - s_{c,k,l}^{(n)}) \right)^H \right. \\ &\quad \left. \times \left(d_{c,k}^{-\zeta} \sum_{i=1, i \neq k}^K \|\mathbf{h}_k^T \mathbf{w}_{c,i}\|^2 + \sigma_{\eta}^2 \right)^{-1} \left(\mathbf{h}_k^T \mathbf{w}_{c,k} (s_{c,k,l}^{(m)} - s_{c,k,l}^{(n)}) \right) \right), \end{aligned} \quad (25)$$

where $\lambda = \sum_{m=1}^M \sum_{\substack{n=1 \\ n \neq m}}^M |s_{c,k,l}^{(n)} - s_{c,k,l}^{(m)}|^2$ and $|s_{c,k,l}^{(n)} - s_{c,k,l}^{(m)}|^2 = \lambda/(M(M-1))$, substituting it in the KLD expression which becomes,

$$\text{KLD}_{c,k} = \frac{\lambda d_{c,k}^{-\zeta}}{2M(M-1) \ln 2} \times \frac{\|\mathbf{h}_k^T \mathbf{w}_{c,k}\|^2}{d_{c,k}^{-\zeta} \sum_{i=1, i \neq k}^K \|\mathbf{h}_k^T \mathbf{w}_{c,i}\|^2 + \sigma_{\eta}^2}. \quad (26)$$

It should be noted that the second term in this equation, represents the form of the SINR, where the interference is the sum of IUI and radar interference.

IV. RADAR SYSTEM ANALYSIS

A. Composite detection and response matrix estimation

The main objective of typical radar systems is to detect targets and estimate the matrix response for each one. After separating signals associated with different targets, we formulate a composite detection-estimation problem as follows,

$$\{\hat{\mathbf{H}}_t, \hat{\mathcal{H}}_q\} = \arg \max_{\mathbf{H}_t, \mathcal{H}_q} \max_{\forall q \in \{0,1\}} f(\mathbf{y}_{r,t,l}; \mathbf{H}_t, \mathbf{x}_t, \mathcal{H}_q). \quad (27)$$

This joint optimisation problem aims to simultaneously detect the presence of a target (determining $\hat{\mathcal{H}}_q$) and estimate its response matrix ($\hat{\mathbf{H}}_t$) if present. For the hypotheses \mathcal{H}_0 and \mathcal{H}_1 , the PDF of the received signals vector $\mathbf{y}_{r,t,l}$ under each hypothesis can be shown as a multivariate normal density,

$$f(\mathbf{y}_{r,t,l}; \mathbf{H}_t, \mathbf{x}_t, \mathcal{H}_q) = \frac{1}{\pi^N [(1-q)\sigma_n^{2N} + q \det(\mathbf{R}_{1,t})]} \times \exp\left(-\mathbf{y}_{r,t,l}^H [(1-q)\sigma_n^{-2} + q \det(\mathbf{R}_{1,t})] \mathbf{y}_{r,t,l}\right), \quad (28)$$

where $\mathbf{R}_{1,t} = \mathbf{H}_t \mathbf{R}_{t,l} \mathbf{H}_t^H + \sigma_n^2 \mathbf{I}_N$, and $\mathbf{R}_{t,l} = \mathbf{x}_{t,l} \mathbf{x}_{t,l}^H d_{r,t,l}^\zeta$. The generalised likelihood ratio test (GLRT) for the t -th target is used to determine target existence or absence by comparing the likelihoods under the two hypotheses, derived as,

$$\Lambda_{t,l} = \frac{\arg \max_{\mathbf{H}_t} f(\mathbf{y}_{r,t,l}; \mathbf{H}_t, \mathbf{x}_t, \mathcal{H}_1)}{\arg \max_{\mathbf{H}_t} f(\mathbf{y}_{r,t,l}; \mathcal{H}_0)}. \quad (29)$$

As the PDF does not depend on \mathbf{H}_t under \mathcal{H}_0 , the target response matrix is estimated under \mathcal{H}_1 , thus by using the maximum likelihood estimation theorem we obtain,

$$\hat{\mathbf{H}}_t = \arg \max_{\mathbf{H}_t} f(\mathbf{y}_{r,t,l}; \mathbf{H}_t, \mathbf{x}_t, \mathcal{H}_1). \quad (30)$$

The likelihood function is Gaussian, and the maximisation leads to the least squares solution,

$$\hat{\mathbf{H}}_t = \arg \min_{\mathbf{H}_t} \|\mathbf{y}_{r,t} - \mathbf{H}_t \mathbf{x}_t\|^2 = \mathbf{y}_{r,t} \mathbf{x}_t^H (\mathbf{x}_t \mathbf{x}_t^H)^{-1}. \quad (31)$$

This least squares solution provides an unbiased estimate of \mathbf{H}_t . Substituting the PDF in (28) into the GLRT, we obtain,

$$\Lambda(\mathbf{y}_{r,t,l}) = \frac{\pi^N \sigma_n^{2N} \exp\left(-(\mathbf{y}_{r,t,l} - \hat{\mathbf{H}}_t \mathbf{x}_t)^H \hat{\mathbf{R}}_{1,t}^{-1} (\mathbf{y}_{r,t,l} - \hat{\mathbf{H}}_t \mathbf{x}_t)\right)}{\pi^N \det(\hat{\mathbf{R}}_{1,t}) \exp\left(-\frac{1}{\sigma_n^2} \mathbf{y}_{r,t,l}^H \mathbf{y}_{r,t,l}\right)} \underset{\mathcal{H}_0}{\overset{\mathcal{H}_1}{\gtrless}} \tau_0 \quad (32)$$

where $\hat{\mathbf{R}}_{1,t} = \hat{\mathbf{H}}_t \mathbf{R}_{t,l} \hat{\mathbf{H}}_t^H + \sigma_n^2 \mathbf{I}_N$ and τ_0 is the detection threshold. Taking the logarithm and rearranging, we obtain,

$$\ln \Lambda(\mathbf{y}_{r,t,l}) = \frac{1}{\sigma_n^2} \mathbf{y}_{r,t,l}^H \mathbf{y}_{r,t,l} - N \ln \sigma_n^2 + \ln \det(\hat{\mathbf{R}}_{1,t}) - (\mathbf{y}_{r,t,l} - \hat{\mathbf{H}}_t \mathbf{x}_t)^H \hat{\mathbf{R}}_{1,t}^{-1} (\mathbf{y}_{r,t,l} - \hat{\mathbf{H}}_t \mathbf{x}_t) \underset{\mathcal{H}_0}{\overset{\mathcal{H}_1}{\gtrless}} \ln \tau_0 \quad (33)$$

The terms $N \ln \sigma_n^2$ and $\ln \det(\hat{\mathbf{R}}_{1,t})$ are constant with respect to $\mathbf{y}_{r,t,l}$, so they can be absorbed into the threshold, which further simplifies our GLRT as follows,

$$\hat{\Lambda}(\mathbf{y}_{r,t,l}) = \mathbf{y}_{r,t,l}^H \left(\mathbf{I}_N + \hat{\mathbf{R}}_{1,t}^{-1}\right) \mathbf{y}_{r,t,l} \underset{\mathcal{H}_0}{\overset{\mathcal{H}_1}{\gtrless}} \tau_1 \quad (34)$$

where $\tau_1 = \ln \tau_0 + N \ln \sigma_n^2 - \ln \det(\hat{\mathbf{R}}_{1,t})$. This expression compares hypotheses \mathcal{H}_0 and \mathcal{H}_1 , incorporating the estimated target response matrix $\hat{\mathbf{H}}_t$ in the covariance matrix $\mathbf{R}_{1,t}$. To use all L snapshots with independent signals, we average as,

$$\bar{\Lambda}_{t,l} = \frac{1}{L} \sum_{l=1}^L \hat{\Lambda}_{t,l} \underset{\mathcal{H}_0}{\overset{\mathcal{H}_1}{\gtrless}} \tau_2. \quad (35)$$

where τ_2 is the detection threshold considering all snapshots and can be designed per the Neyman-Pearson lemma.

B. The KLD of radar system

As the number of snapshots L approaches infinity, the law of large numbers ensures that the estimated target response matrix converges in probability to the true value, i.e., $\hat{\mathbf{H}}_t \xrightarrow{P} \mathbf{H}_t$. This allows us to use \mathbf{H}_t in place of $\hat{\mathbf{H}}_t$ for large L . Under this assumption, we can proceed with a more tractable derivation of the KLD for the radar subsystem.

Using this property, we can now derive the $\text{KLD}_{r,t}^{\mathcal{H}_0 \rightarrow \mathcal{H}_1}$ for the radar subsystem using the probability density functions established in (28), and (7) as follows,

$$\text{KLD}_{r,t}^{\mathcal{H}_0 \rightarrow \mathcal{H}_1} = \frac{1}{\ln 2} \left(\ln \det(\mathbf{R}_{2,t}) + \text{Tr}(\mathbf{R}_{2,t}^{-1} (\sigma_n^2 \mathbf{I}_N)) - N (1 + \ln(\sigma_n^2)) \right), \quad (36)$$

where $\mathbf{R}_{2,t} = \frac{1}{L} \sum_{l=1}^L \mathbf{R}_{1,t} = \mathbf{H}_t \frac{1}{L} \sum_{l=1}^L \mathbf{R}_{t,l} \mathbf{H}_t^H + \sigma_n^2 \mathbf{I}_N = \mathbf{H}_t \mathbf{R}_t \mathbf{H}_t^H + \sigma_n^2 \mathbf{I}_N$, and $\det(\cdot)$ is the determinant operation. $\text{KLD}_{r,t} = \frac{1}{2} \left(\text{KLD}_{r,t}^{\mathcal{H}_0 \rightarrow \mathcal{H}_1} + \text{KLD}_{r,t}^{\mathcal{H}_1 \rightarrow \mathcal{H}_0} \right)$, where in this case $\text{KLD}_{r,t}^{\mathcal{H}_0 \rightarrow \mathcal{H}_1} = \text{KLD}_{r,t}^{\mathcal{H}_1 \rightarrow \mathcal{H}_0}$.

V. RADAR WAVEFORM OPTIMISATION

In this section, the radar waveform is optimised while using the ZF beamforming scheme for the communication subsystem. The optimisation problem is,

$$\mathcal{P}_1 : \max_{\mathbf{W}_r} \frac{1}{T} \sum_{t=1}^T \text{KLD}_{r,t} |_{\mathbf{W}_{r,t}, \mathbf{H}_t} \quad (37a)$$

$$\text{s.t. } \underline{A}_t \leq \text{KLD}_{r,t}, \quad \forall t \in T, \quad (37b)$$

$$\underline{B}_k \leq \text{KLD}_{c,k}, \quad \forall k \in K, \quad (37c)$$

$$\sum_{t=1}^T \frac{1}{L} \|\mathbf{W}_{r,t}\|_F^2 \leq P_r, \quad (37d)$$

$$P_c = P_T - P_r, \quad (37e)$$

where $\text{KLD}_{r,t} |_{\mathbf{W}_{r,t}, \mathbf{H}_t}$ is defined in (36). After substituting (36) in (37a), can be written as \mathcal{P}_2 that is given on page 7. This optimisation problem focuses on the radar waveform while considering the whole ISAC system performance. The constraint on radar power (37d) is explicit because the radar waveform is our primary optimisation variable. The communication power is implicitly considered through the ZF beamforming scheme and the constraint (37c) on communication performance. Specifically, the communication subsystem utilises its allocated power through the ZF beamforming scheme to distribute power to each UE, with weights predetermined based on the channel state information.

To solve the optimisation problem in (38), we utilise the Projected Gradient method with a penalty function [36]. This

$$\begin{aligned} \mathcal{P}_2 : \max_{\dot{\mathbf{W}}_r} & \frac{1}{T} \sum_{t=1}^T \frac{1}{\ln 2} \left(\ln \left(\det \left(d_{r,t}^{\zeta} \mathbf{H}_t \left(\frac{1}{L} \mathbf{W}_{r,t} \mathbf{W}_{r,t}^H + \mathbf{W}_c \mathbf{W}_c^H \right) \mathbf{H}_t^H + \sigma_n^2 \mathbf{I}_N \right) \right) \right. \\ & \left. + \text{Tr} \left(\left(d_{r,t}^{\zeta} \mathbf{H}_t \left(\frac{1}{L} \mathbf{W}_{r,t} \mathbf{W}_{r,t}^H + \mathbf{W}_c \mathbf{W}_c^H \right) \mathbf{H}_t^H + \sigma_n^2 \mathbf{I}_N \right)^{-1} (\sigma_n^2 \mathbf{I}_N) \right) - N (1 + \ln(\sigma_n^2)) \right) \end{aligned} \quad (38)$$

s.t. (37b), (37c), (37d), and (37e)

method is chosen for its suitability to the non-linear, non-convex optimisation problem [37]. This method uses a penalty function for KLD constraints and handles radar power via projection, balancing the solution quality and computational efficiency for real-time ISAC applications. Its scalability makes it suitable for radar waveform optimisation in ISAC. The optimisation variable $\dot{\mathbf{W}}_r \in \mathbb{C}^{N \times L \times T}$ is a three-dimensional tensor, where $\mathbf{w}_{r,t,l}$, $\mathbf{W}_{r,t}$, and $\mathbf{W}_{r,l}$ are all parts of this tensor. We define the objective function $f(\dot{\mathbf{W}}_r)$ and a penalty function $p(\dot{\mathbf{W}}_r)$ to handle the constraints in (37b) and (37c),

$$f(\dot{\mathbf{W}}_r) = \frac{1}{T} \sum_{t=1}^T \text{KLD}_{r,t|\mathbf{W}_{r,t},\mathbf{H}_t}, \quad (39)$$

$$\begin{aligned} p(\dot{\mathbf{W}}_r) &= \sum_{t=1}^T \left(\max(0, \underline{A}_t - \text{KLD}_{r,t|\mathbf{W}_{r,t},\mathbf{H}_t})^2 \right) \\ &+ \sum_{k=1}^K \left(\max(0, \underline{B}_k - \text{KLD}_{c,k|\dot{\mathbf{W}}_r})^2 \right). \end{aligned} \quad (40)$$

The gradient of the objective function, $\nabla f(\dot{\mathbf{W}}_r) \in \mathbb{C}^{N \times L \times T}$, is a gradient tensor computed element-wise, as detailed in Appendix I.A. The final equation is given by,

$$\begin{aligned} [\nabla f(\dot{\mathbf{W}}_r)]_{i,l,t} &= \frac{2 d_{r,t}^{\zeta}}{TL \ln 2} \left(\mathbf{H}_t^H (\mathbf{R}_{2,t})^{-1} \mathbf{H}_t \mathbf{W}_{r,t} \right. \\ &\left. - \sigma_n^2 (\mathbf{R}_{2,t})^{-2} \mathbf{H}_t \mathbf{W}_{r,t} \right)_i. \end{aligned} \quad (41)$$

The gradient of the penalty function $\nabla p(\dot{\mathbf{W}}_r) \in \mathbb{C}^{N \times L \times T}$ is also a gradient tensor, computed as,

$$\begin{aligned} [\nabla p(\dot{\mathbf{W}}_r)]_{i,l,t} &= -2(\underline{A}_t - \text{KLD}_{r,t})[\nabla \text{KLD}_{r,t}]_{i,l} \cdot \mathbb{I}_1 \\ &- \sum_{k=1}^K 2(\underline{B}_k - \text{KLD}_{c,k})[\nabla \text{KLD}_{c,k}]_{i,l,t} \cdot \mathbb{I}_2, \end{aligned} \quad (42)$$

where $\mathbb{I}_1 = \mathbb{I}(\text{KLD}_{r,t} < \underline{A}_t)$ and $\mathbb{I}_2 = \mathbb{I}(\text{KLD}_{c,k} < \underline{B}_k)$ with $\mathbb{I}(\cdot)$ represents the indicator function. The gradients of KLD_r and KLD_c with respect to $\mathbf{W}_{r,t}$ and $\dot{\mathbf{W}}_r$, respectively, are provided in Appendix I.A. The final forms are given by,

$$\begin{aligned} [\nabla \text{KLD}_{r,t|\mathbf{W}_{r,t},\mathbf{H}_t}]_{i,l} &= \frac{2 d_{r,t}^{\zeta}}{L \ln 2} \left(\mathbf{H}_t^H \mathbf{R}_{2,t}^{-1} \mathbf{H}_t \mathbf{W}_{r,t} \right. \\ &\left. - \sigma_n^2 \mathbf{H}_t^H \mathbf{R}_{2,t}^{-2} \mathbf{H}_t \mathbf{W}_{r,t} \right)_i, \end{aligned} \quad (43)$$

$$[\nabla \text{KLD}_{c,k|\dot{\mathbf{W}}_r,\mathbf{H}_t}]_{i,l,t} = -\frac{2 d_{c,k}^{\zeta} \lambda p_k (N-K) \sigma_n^2}{M(M-1) L \sigma_n^2 \ln 2} [\dot{\mathbf{W}}_r]_{i,l,t}. \quad (44)$$

The update rule for the projected gradient method with penalty ensures that each iteration moves the solution towards optimality while maintaining feasibility, and can be shown as follows,

$$\dot{\mathbf{W}}_r^{(n+1)} = \mathcal{P} \left(\dot{\mathbf{W}}_r^{(n)} + \alpha_n \mathbf{G}^{(n)} \right), \quad (45)$$

Algorithm 1 Projected Gradient Method with Penalty for Radar Waveform Optimisation

Require: Initial point $\dot{\mathbf{W}}_r^{(0)}$, constants $\alpha_0, \rho_0, \beta, \gamma, c, P_r, \underline{A}_t, \underline{B}_k$, tolerance ε , and maximum iterations `max_iter`

Ensure: Optimal solution $\dot{\mathbf{W}}_r^*$

- 1: Initialise $n = 0$
 - 2: **while** $n < \text{max_iter}$ **do**
 - 3: Compute gradients $\nabla f(\dot{\mathbf{W}}_r^{(n)})$ and $\nabla p(\dot{\mathbf{W}}_r^{(n)})$
 - 4: Compute total gradient $\mathbf{G}^{(n)} = \nabla f(\dot{\mathbf{W}}_r^{(n)}) - \rho_n \nabla p(\dot{\mathbf{W}}_r^{(n)})$
 - 5: Perform backtracking line search to find α_n
 - 6: Update $\dot{\mathbf{W}}_r^{(n+1)} = \mathcal{P}(\dot{\mathbf{W}}_r^{(n)} + \alpha_n \mathbf{G}^{(n)})$
 - 7: Compute $f(\dot{\mathbf{W}}_r^{(n+1)})$ and $p(\dot{\mathbf{W}}_r^{(n+1)})$
 - 8: Update ρ_{n+1} according to the penalty update rule
 - 9: **if** $\|\dot{\mathbf{W}}_r^{(n+1)} - \dot{\mathbf{W}}_r^{(n)}\|_F < \varepsilon$ **then**
 - 10: **break**
 - 11: **end if**
 - 12: $n = n + 1$
 - 13: **end while**
 - 14: **return** $\dot{\mathbf{W}}_r^* = \dot{\mathbf{W}}_r^{(n)}$
-

where $\mathbf{G}^{(n)} = \nabla f(\dot{\mathbf{W}}_r^{(n)}) - \rho_n \nabla p(\dot{\mathbf{W}}_r^{(n)})$ is the gradient direction, combining the objective function gradient and the penalty function gradient, ρ_n is the penalty parameter, balancing the objective and constraint satisfaction, α_n is the step size, and \mathcal{P} is the projection onto the feasible set defined by the power constraint, ensuring that the power constraint in (37d) is always satisfied. The projection mechanism is shown as,

$$\mathcal{P}(\dot{\mathbf{W}}_r) = \begin{cases} \dot{\mathbf{W}}_r \sqrt{\frac{P_r L}{\|\dot{\mathbf{W}}_r\|_F^2}}, & \text{if } \frac{1}{L} \|\dot{\mathbf{W}}_r\|_F^2 > P_r \\ \dot{\mathbf{W}}_r, & \text{otherwise} \end{cases} \quad (46)$$

The step size α_n is determined using a backtracking line search to ensure convergence. We find the smallest non-negative integer m such that,

$$\begin{aligned} f(\dot{\mathbf{W}}_r^{(n+1)}) - \rho_n p(\dot{\mathbf{W}}_r^{(n+1)}) &\geq \\ f(\dot{\mathbf{W}}_r^{(n)}) - \rho_n p(\dot{\mathbf{W}}_r^{(n)}) + c \alpha_n \|\mathbf{G}^{(n)}\|_F^2, \end{aligned} \quad (47)$$

where $c \in (0, 1)$. This condition, known as the Armijo condition, ensures a sufficient decrease in the penalised objective function [38]. The step size is set as $\alpha_n = \beta^m \alpha_{n-1}$, with $\beta \in (0, 1)$ as a reduction factor. The penalty parameter ρ_n is updated as follows,

$$\rho_{n+1} = \begin{cases} \gamma \rho_n, & \text{if } p(\dot{\mathbf{W}}_r^{(n+1)}) > 0 \\ \rho_n, & \text{otherwise} \end{cases} \quad (48)$$

where $\gamma > 1$ is a constant factor. This adaptive scheme increases the penalty when constraints are violated and keeps it constant when they are satisfied. The projection operator \mathcal{P} ensures that the power constraint is always satisfied. The backtracking line search procedure is used to determine an

appropriate step size α_n at each iteration. This adaptive step size selection helps to ensure a sufficient increase in the objective function while maintaining the stability of the algorithm. The line search condition can be expressed as,

$$\phi(\dot{\mathbf{W}}_r^{(n+1)}) \leq \phi(\dot{\mathbf{W}}_r^{(n)}) + c\alpha_n \langle \nabla \phi(\dot{\mathbf{W}}_r^{(n)}), \dot{\mathbf{W}}_r^{(n+1)} - \dot{\mathbf{W}}_r^{(n)} \rangle, \quad (49)$$

where $\phi(\dot{\mathbf{W}}_r) = f(\dot{\mathbf{W}}_r) - \rho_n p(\dot{\mathbf{W}}_r)$ is the penalised objective function. The penalty parameter ρ_n is updated adaptively based on the constraint violation, allowing the algorithm to balance optimisation and constraint satisfaction. If constraints are consistently violated, the increasing penalty will emphasise constraint adherence.

VI. COMMUNICATION OPTIMISATION

The communication subsystem optimisation uses the gradient-assisted IPM [39], in contrast to the projected gradient method with penalty used for radar optimisation, due to the different optimisation variable structures. Radar optimisation involves a three-dimensional tensor $\dot{\mathbf{W}}_r \in \mathbb{C}^{N \times L \times T}$, while communication beamforming optimises a two-dimensional matrix $\mathbf{W}_c \in \mathbb{C}^{N \times K}$. This reduced dimensionality makes IPM particularly suitable, potentially offering faster convergence and more precise solutions. The communication waveform is optimised while using the conventional identity covariance matrix design for the radar subsystem, with $\mathbf{R}_w = \mathbf{I}_{N \times N} \quad \forall t \in T$. The optimisation problem can be expressed as follows,

$$\mathcal{P}_3 : \max_{\mathbf{W}_c} \frac{1}{K} \sum_{k=1}^K \text{KLD}_{c,k} | \mathbf{W}_c, \mathbf{h}_k \quad (50a)$$

$$\text{s.t. } \underline{A}_t \leq \text{KLD}_{r,t}, \quad \forall t \in T, \quad (50b)$$

$$\underline{B}_k \leq \text{KLD}_{c,k}, \quad \forall k \in K, \quad (50c)$$

$$\|\mathbf{W}_c\|_F^2 \leq P_c, \quad (50d)$$

$$P_r = P_T - P_c. \quad (50e)$$

Note, that the radar power is uniformly distributed among potential targets, as the radar covariance matrix ensures omnidirectional beam flow. To solve this optimisation problem, we must derive the gradients of the objective function and the constraints. Let's define the objective function as follows,

$$f(\mathbf{W}_c) = \frac{1}{K} \sum_{k=1}^K \text{KLD}_{c,k} | \mathbf{W}_c, \mathbf{h}_k. \quad (51)$$

To compute the gradient of the objective function, we need to derive the gradients of each component of \mathbf{W}_c . Let $a_k = d_{c,k}^\zeta |\mathbf{h}_k^T \mathbf{w}_{c,k}|^2$. Using the chain rule and properties of matrix derivatives, the gradients can be expressed as follows,

$$\nabla_{\mathbf{w}_{c,j}} |\mathbf{h}_k^T \mathbf{w}_{c,j}|^2 = 2d_{c,k}^\zeta \mathbf{h}_k \mathbf{h}_k^T \mathbf{w}_{c,j} \quad \text{for all } j \quad (52)$$

$$\nabla_{\mathbf{w}_{c,j}} \text{KLD}_{c,k} = \begin{cases} C \cdot \frac{2d_{c,k}^\zeta \mathbf{h}_k \mathbf{h}_k^T \mathbf{w}_{c,k}}{b_k}, & \text{if } j = k \\ -C \cdot \frac{2d_{c,k}^\zeta \mathbf{h}_k \mathbf{h}_k^T \mathbf{w}_{c,j} \cdot a_k}{b_k^2}, & \text{if } j \neq k \end{cases} \quad (53)$$

Algorithm 2 Interior Point Method for Communication Optimisation

Require: Initial point $\mathbf{W}_c^{(0)}$, constants $\mu_0, \gamma, P_c, \underline{A}_t, \underline{B}_k$, tolerance ϵ , and maximum iterations `max_iter`

Ensure: Optimal solution \mathbf{W}_c^*

- 1: Initialise $n = 0, \mu = \mu_0$
 - 2: **while** $n < \text{max_iter}$ **do**
 - 3: Compute $f(\mathbf{W}_c^{(n)}), \nabla f(\mathbf{W}_c^{(n)}), g_i(\mathbf{W}_c^{(n)})$, and $\nabla g_i(\mathbf{W}_c^{(n)})$
 - 4: Compute KKT conditions
 - 5: **if** KKT conditions satisfied within ϵ **then**
 - 6: **break**
 - 7: **end if**
 - 8: Solve Newton system for search direction $\Delta \mathbf{W}_c$
 - 9: Perform line search to find step size α
 - 10: Update $\mathbf{W}_c^{(n+1)} = \mathbf{W}_c^{(n)} + \alpha \Delta \mathbf{W}_c$
 - 11: Update $\mu = \gamma \mu$
 - 12: $n = n + 1$
 - 13: **end while**
 - 14: **return** $\mathbf{W}_c^* = \mathbf{W}_c^{(n)}$
-

where $C = \frac{\lambda}{2M(M-1) \ln 2}$, and $b_k = d_{c,k}^\zeta \sum_{i=1, i \neq k}^K \|\mathbf{h}_k^T \mathbf{w}_{c,i}\|^2 + \sigma_\eta^2$. Finally, we can express the gradient of the objective function as,

$$\nabla_{\mathbf{w}_{c,k}} f(\mathbf{W}_c) = \frac{d_{c,k}^\zeta C}{K} \sum_{k=1}^K \left(\frac{2\mathbf{h}_k \mathbf{h}_k^T \mathbf{w}_{c,k}}{b_k} - \sum_{j \neq k} \frac{2\mathbf{h}_k \mathbf{h}_k^T \mathbf{w}_{c,j} \cdot a_k}{b_k^2} \right). \quad (54)$$

Next, we need to consider the constraints of our optimisation problem. The power constraint is given by,

$$g(\mathbf{W}_c) = \|\mathbf{W}_c\|_F^2 - P_c \leq 0. \quad (55)$$

The gradient of this constraint is derived as follows,

$$\nabla_{\mathbf{w}_{c,j}} g(\mathbf{W}_c) = 2\mathbf{w}_{c,j}. \quad (56)$$

The gradient of the radar KLD constraint with respect to \mathbf{W}_c is derived as follows,

$$\nabla_{\mathbf{W}_c} \text{KLD}_{r,t} = \frac{d_{r,t}^\zeta}{\ln 2} (\mathbf{R}_{2,t}^{-1} \mathbf{H}_t \mathbf{W}_c \mathbf{H}_t^H). \quad (57)$$

Solving the optimisation problem defined in equations (50a)-(50d) uses the IPM, as detailed in **Algorithm 2**. This method efficiently addresses constrained optimisation with key parameters: an initial barrier parameter $\tilde{\mu}_0$, a barrier reduction factor $\tilde{\gamma}$, and a convergence tolerance ϵ . The algorithm iteratively computes the objective function, constraints, and their gradients, checks the Karush-Kuhn-Tucker (KKT) conditions and updates the solution using a Newton system and line search. The barrier parameter $\tilde{\mu}$ is updated as $\tilde{\mu} = \tilde{\gamma} \tilde{\mu}$ in each iteration, gradually enforcing constraints more strictly. This continues until $|\mathbf{W}_c^{(n+1)} - \mathbf{W}_c^{(n)}|_F < \epsilon$ or the maximum iterations are reached, yielding the optimal beamforming matrix \mathbf{W}_c^* that maximises the communication KLD while satisfying radar and power constraints.

VII. NUMERICAL RESULTS

In this section, we present simulation results for our conventional benchmarks and the two previously introduced optimisation techniques. The total transmit power is fixed at $P_T = 1$, and QPSK modulation is used throughout. The base station has $N = 20$ antennas, with $L = 100$ snapshots, a maximum of $T = 3$ potential radar targets, and $K = 3$ UEs. The pathloss exponent is $\eta = 3$ to model large-scale fading. The distances from the BS to the UEs are $d_{c,k} = \{150, 210, 100\} \forall k \leq K$ meters and to the targets are $d_{r,t} = \{100, 115, 95\} \forall t \leq T$ meters. The channel variance is $\sigma_h^2 = 1$.

A. Trade-off for the conventional benchmarks

The radar subsystem employs a conventional identity covariance matrix design, with $\mathbf{R}_w = \mathbf{I}_N$, while the communication subsystem utilises the previously introduced MRT and ZF.

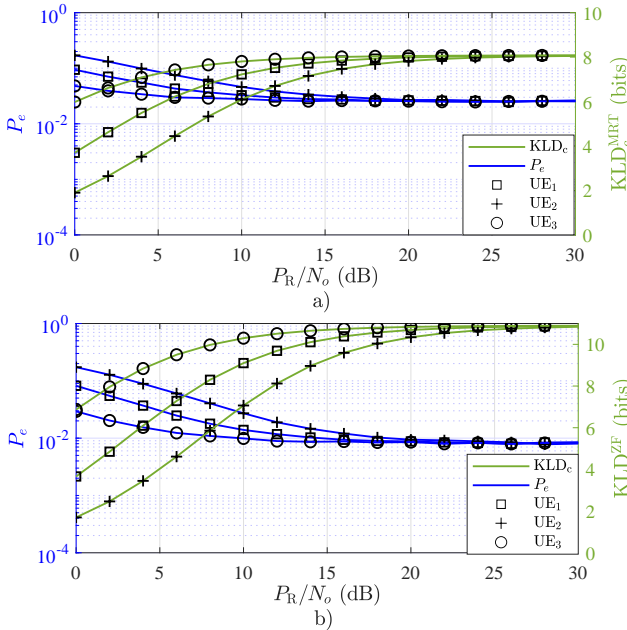


Fig. 1. Performance of the communication subsystem for both beamforming schemes, showing BER and achievable KLD_c versus P_R/N_o with $P_T = 0.5$.

Fig. 1 shows the communication subsystem performance for both ZF and MRT beamforming. In Fig. 1.a, the MRT scheme's performance is illustrated, with KLD on the right y -axis and BER on the left. The KLD values for all UEs increase with P_R/N_o up to about 10 dB, where an upper bound appears due to radar interference, with IUI contributing less significantly. Similarly, the BER decreases with P_R/N_o , reflecting improved communication performance but also reaches an error floor around 10 dB. Fig. 1.b presents the ZF scheme's performance, showing similar KLD and BER trends. However, the ZF scheme exhibits higher KLD values and lower BER values for the same received SNR compared to MRT, confirming that radar interference is the primary source, as IUI is cancelled using ZF precoding. Both schemes display a significant error floor in BER and an upper bound in KLD due to persistent radar interference at $P_c = 0.5$. This figure effectively demonstrates the utility of KLD in characterising the communication system.

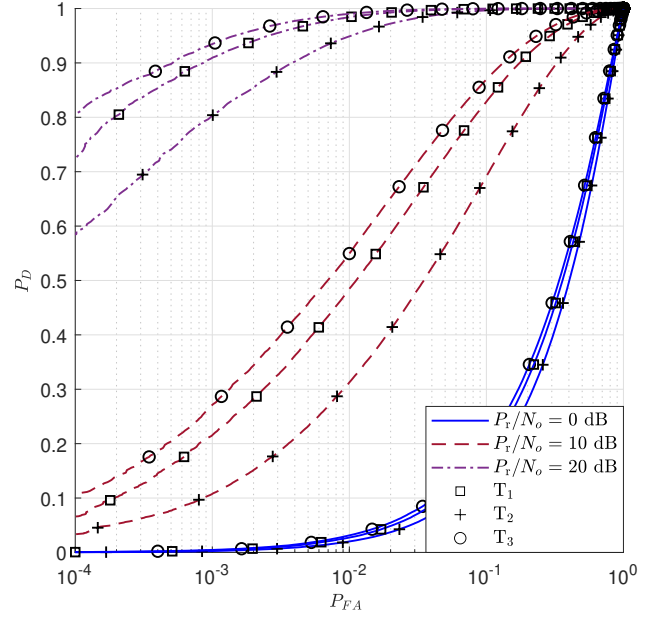


Fig. 2. The ROC curves depict the performance for the three targets across different P_R/N_o scenarios.

Fig. 2 presents the receiver operating characteristic (ROC) curves for the radar subsystem's performance across three potential targets at varying P_R/N_o levels, using ZF precoding for the communication subsystem as shown in Fig. 1. The ROC curves plot the probability of detection (P_D) against the probability of false alarm (P_{FA}) for each target. At $P_R/N_o = 0$ dB, the ROC curves for targets T₁, T₂, and T₃ are closely aligned, indicating similar detection performance at low SNR. However, at $P_R/N_o = 10$ dB, the curves diverge, with T₃ showing the best performance, followed by T₁ and T₂. This trend continues at $P_R/N_o = 20$ dB, where the separation is even more pronounced. Notably, at $P_{FA} = 10^{-3}$, the P_D values are $\{0.909, 0.804, 0.935\}$ for T₁, T₂, and T₃, respectively. T₃ remains the most detectable, while both T₂ and T₁ show significant detection improvements compared to lower P_R/N_o scenarios. This illustrates that higher SNR enhances the radar subsystem's capability to detect and differentiate targets effectively.

In Fig. 3.a, the radar subsystem performance is illustrated through the achievable KLD_r of each target versus P_R/N_o for varying P_T . As P_R/N_o increases, the achievable KLD_r also improves, indicating enhanced radar performance. The performance curves for different P_T values are close, suggesting that the system is less sensitive to P_T changes due to the communication signal's incorporation in target detection using our improved system model. Fig. 3.b presents the trade-off performance between both subsystems using ZF and MRT for communication, along with the conventional identity covariance design for radar. The plot shows KLD_c versus KLD_r at equal power allocation, with each point representing a different P_R/N_o value going higher from left to right. The KLD_c^{ZF} slightly outperforms KLD_c^{MRT}, both exhibiting saturation at higher P_R/N_o due to radar interference, while KLD_r steadily increases along the curve. Notably, a KLD_c^{ZF} of 8 bits is achieved at $P_R/N_o = 12$ dB for UE₂, whereas the same KLD_c^{MRT} requires around 25 dB, implying an SNR gain of

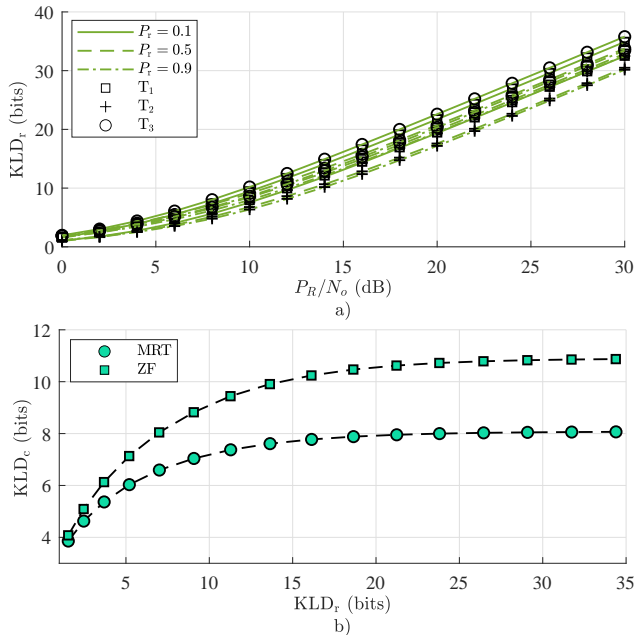


Fig. 3. a) Radar subsystem performance: achievable KLD_r versus P_R/N_o for varying P_r . b) KLD trade-off between subsystems for ZF and MRT.

about 13 dB in favor of ZF.

B. Radar Waveform KLD-based Optimisation

The radar waveform KLD-based optimisation algorithm is set with a maximum of $\max_iter = 1000$, convergence tolerance $\epsilon = 10^{-6}$, initial penalty $\rho_0 = 1$, penalty increase $\gamma = 1.5$, and initial step size $\alpha_0 = 0.1$. The KLD lower bounds \underline{A}_t and \underline{B}_k for all targets and UEs are 10 bits.

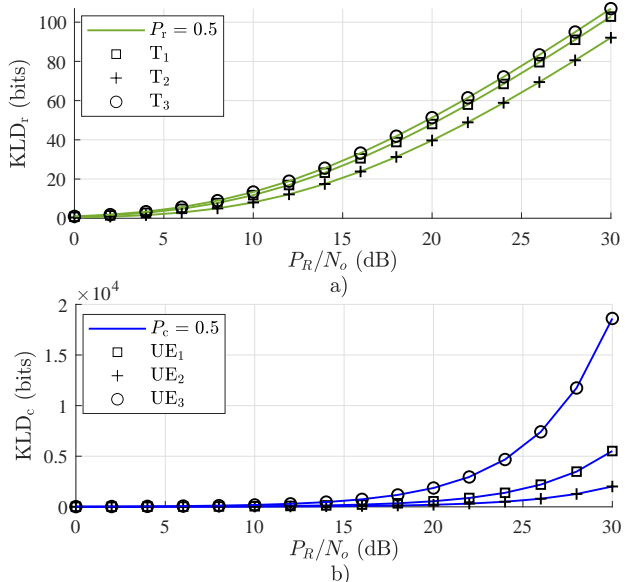


Fig. 4. The performance of both subsystems using optimised radar waveform. a) KLD_r versus P_R/N_o ; b) KLD_c versus P_R/N_o .

Fig. 4 illustrates the performance of both subsystems with the optimised radar waveform. In Fig. 4.a, the achievable KLD_r for each target versus P_R/N_o is shown. As P_R/N_o increases, KLD_r improves for all targets, indicating enhanced radar performance. T_3 consistently achieves the highest

KLD_r , followed by T_1 and T_2 , reflecting their distances from the BS. At $P_R/N_o = 10$ dB, the $\{KLD_{r,1}, KLD_{r,2}, KLD_{r,3}\}$ values are approximately $\{11.78, 8.06, 13.38\}$ bits for T_1 , T_2 , and T_3 , increasing to $\{48.06, 39.68, 51.31\}$ bits at $P_R/N_o = 20$ dB. The rate of KLD_r improvement after 15 dB suggests a near-linear relationship with P_R/N_o , indicating consistent performance enhancement in the radar system. Fig. 4.b illustrates the communication subsystem performance, showing KLD_c versus P_R/N_o . For P_R/N_o values between 0-8 dB, KLD_c exhibits minimal improvement, indicating system infeasibility in this low power regime due to the inability to meet minimum KLD requirements for all UEs. UE_3 consistently achieves the highest KLD_c , followed by UE_1 and UE_2 . At $P_R/N_o = 10$ dB, the values $\{KLD_{c,1}, KLD_{c,2}, KLD_{c,3}\}$ are approximately $\{55.14, 20.09, 186.09\}$ for UE_1 , UE_2 , and UE_3 , increasing to $\{551.38, 200.94, 1860.91\}$ at $P_R/N_o = 20$ dB. The sharp increase in KLD_c beyond 8 dB suggests the system has reached its optimisation feasibility point, significantly enhancing the communication performance as the radar interference is effectively reduced. These results highlight the intricate relationship between radar detection capabilities and communication system performance, illustrating how both subsystems benefit once the feasibility threshold is surpassed, with the performance reflecting the respective distances from the BS.

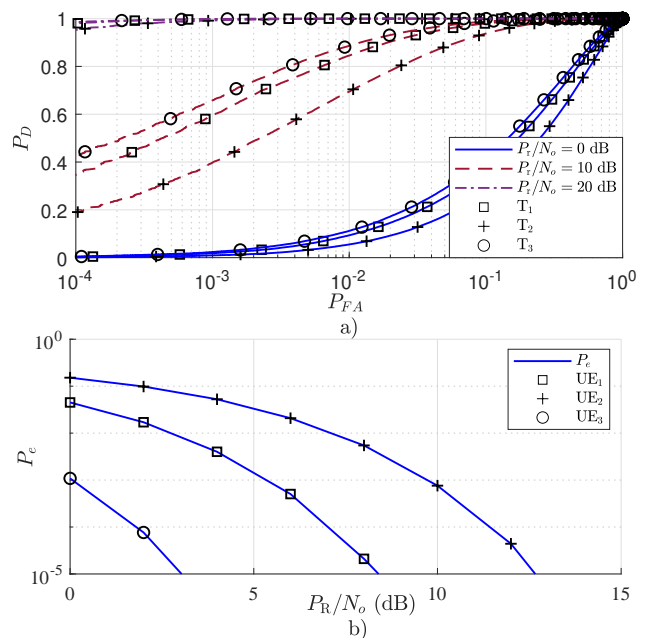


Fig. 5. a) The ROC curves depict the performance for the three targets across different P_R/N_o scenarios. b) The BER versus P_R/N_o .

Fig. 5.a presents the ROC curves for the three targets across different P_R/N_o scenarios. At $P_R/N_o = 20$ dB and $P_{FA} = 10^{-3}$, the P_D is $\{0.997, 0.991, 0.998\}$ for T_1 , T_2 , and T_3 , respectively, compared to $\{0.909, 0.804, 0.935\}$ in the non-optimal case, demonstrating improved detection capabilities through optimisation. Fig. 5.b shows the BER performance for the three UEs versus P_R/N_o . As P_R/N_o increases, BER decreases for all UEs, with UE_3 achieving the lowest BER, followed by UE_2 and UE_1 . The communication subsystem significantly benefits from radar waveform optimisation, as evidenced by the non-optimal case where P_e saturates at

8×10^{-3} after 15 dB, as shown in Fig. 1, while optimised waveforms reduce P_e below 10^{-5} by 13 dB, effectively mitigating radar interference.

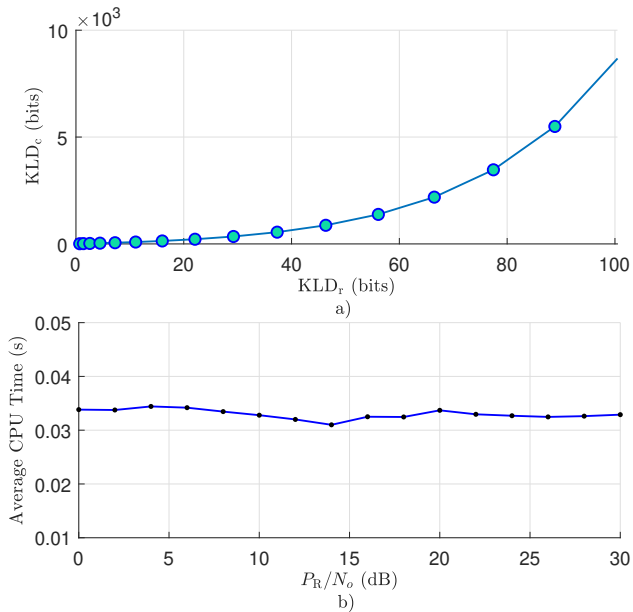


Fig. 6. a) The trade-off performance between the two subsystems KLD_c versus KLD_r. b) The average CPU time (seconds) versus P_R/N_o .

Fig. 6.a illustrates the trade-off performance between both subsystems using the optimised radar waveform, showing KLD_c versus KLD_r for different P_R/N_o values. As P_R/N_o increases, both KLD_c and KLD_r improve, indicating enhanced performance in both subsystems. This highlights the robustness of the optimisation technique in balancing radar and communication performance. In comparison, the non-optimal approach in Fig. 3.b saturates at around 11 bits, indicating an increasing and favourable trade-off for the optimal way. Fig. 6.b presents the average CPU time of the radar waveform optimisation technique versus P_R/N_o . The average CPU time fluctuates slightly between 0.03 and 0.035 seconds, with no clear trend of increase or decrease as P_R/N_o changes, indicating consistent computational efficiency across varying P_R/N_o values, which is beneficial for practical implementation in diverse channel conditions.

C. Communication Waveform KLD-based Optimisation

The communication waveform KLD-based optimisation algorithm is configured similarly to the radar algorithm, with a maximum iteration limit of $\text{max_iter} = 1000$ and a convergence tolerance of $\epsilon = 10^{-6}$. The barrier parameter is initialised at $\tilde{\mu}_0 = 1$ and the barrier reduction factor at $\tilde{\gamma} = 0.1$. The KLD lower bounds for all targets and UEs, \underline{A}_t and \underline{B}_k , are set to 10 bits.

Fig. 7 illustrates the performance of the radar and communication subsystems using the optimised communication waveform. Fig. 7.a shows the achievable KLD_r for each target as a function of P_R/N_o for power allocations of $P_r = \{0.7, 0.5, 0.3\}$. As P_R/N_o increases, KLD_r improves across all targets, with target T₃ consistently achieving the highest KLD_r, followed by T₂ and T₁. For example, at $P_R/N_o =$

10 dB and $P_r = 0.7$, the $\{KLD_{r,1}, KLD_{r,2}, KLD_{r,3}\}$ values are approximately $\{8.42, 10.78, 12.64\}$, increasing to $\{38.26, 42.14, 47.53\}$ at $P_R/N_o = 20$ dB. The linear improvement in KLD_r beyond 15 dB indicates stable radar performance despite the suboptimal waveform. Fig. 7.b depicts the communication subsystem performance with KLD_c versus P_R/N_o for $P_c = \{0.7, 0.5, 0.3\}$. UE₃ achieves the highest KLD_c, followed by UE₂ and UE₁. At $P_R/N_o = 10$ dB and $P_c = 0.7$, the $\{KLD_{c,1}, KLD_{c,2}, KLD_{c,3}\}$ values are approximately $\{45.87, 63.92, 86.14\}$, rising to $\{128.43, 159.47, 182.76\}$ at $P_R/N_o = 20$ dB. The communication performance shows less sharp improvement at higher P_R/N_o due to the need to balance radar subsystem thresholds with communication enhancements across different power allocations.

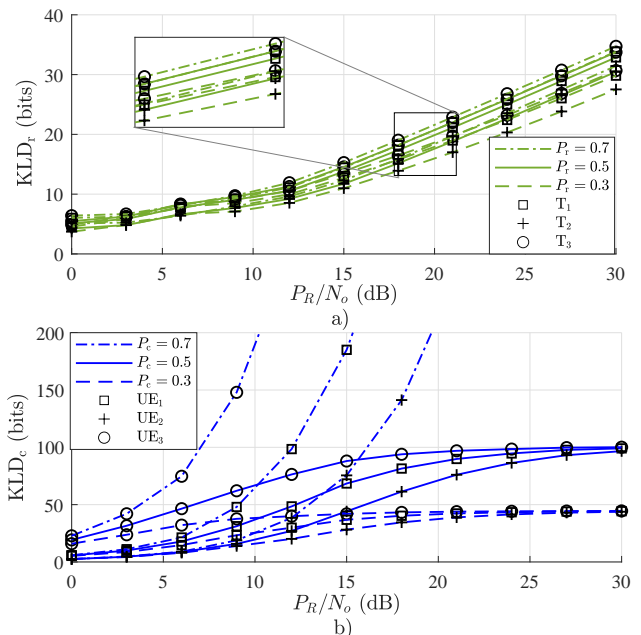


Fig. 7. The performance of both subsystems using optimised communication waveform. a) KLD_r versus P_R/N_o ; b) KLD_c versus P_R/N_o .

Fig. 8.a shows the ROC curves for the three targets at different P_R/N_o levels. At $P_R/N_o = 10$ dB and $P_{FA} = 10^{-3}$, the P_D values are $\{0.397, 0.231, 0.454\}$ for T₁, T₂, and T₃, respectively, compared to $\{0.217, 0.109, 0.273\}$ for the non-optimal case. These results indicate that communication optimisation enhances detection capabilities at lower P_R/N_o compared to non-optimisation, as shown in Fig. 2. Fig. 8.b depicts the BER performance for three UEs versus P_R/N_o . The BER decreases with increasing P_R/N_o , reflecting improved communication performance. UE₃ consistently achieves the lowest BER, followed by UE₂ and UE₁. In the non-optimal scenario, P_e saturates at 8×10^{-3} after 15 dB (Fig. 1), while with optimisation, P_e drops below 10^{-4} by 15 dB across all UEs. Although optimised waveforms provide a performance gain over the non-optimal method, the gain is less pronounced than with optimised radar waveforms due to radar interference.

Fig. 9.a illustrates the trade-off between both subsystems using the optimised communication waveform, showing KLD_c versus KLD_r for different P_R/N_o values. As P_R/N_o increases from left to right, both KLD_c and KLD_r improve, indicating

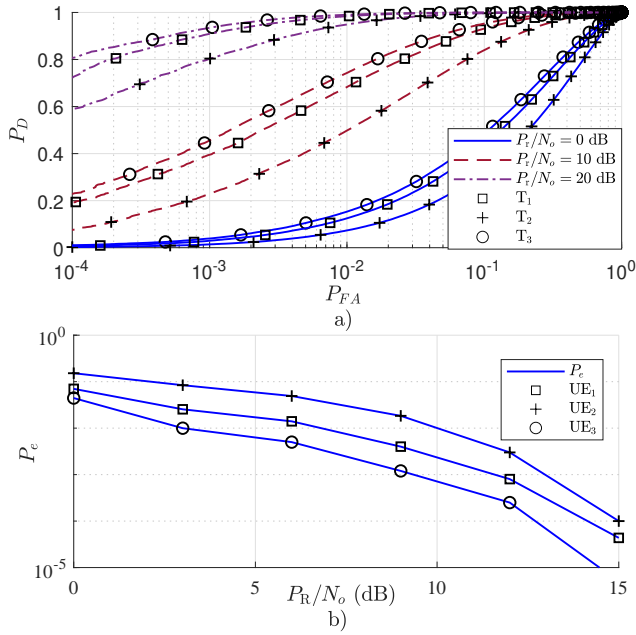


Fig. 8. a) The ROC curves depict the performance for the three targets across different P_R/N_o scenarios. b) The BER versus P_R/N_o .

enhanced performance in both subsystems. This highlights the robustness of the optimisation technique in balancing radar and communication performance. In contrast, the non-optimal case in Fig. 3.b shows KLD_c saturating around 11 bits. Fig. 9.b presents the average CPU time for the communication waveform optimisation technique versus P_R/N_o . The computational complexity stabilises after 15 dB as the ISAC system transitions from an infeasible region, where minimum thresholds cannot be met for all targets and UEs, to a feasible region, with average CPU time fluctuating between 0.02 and 0.04 seconds.

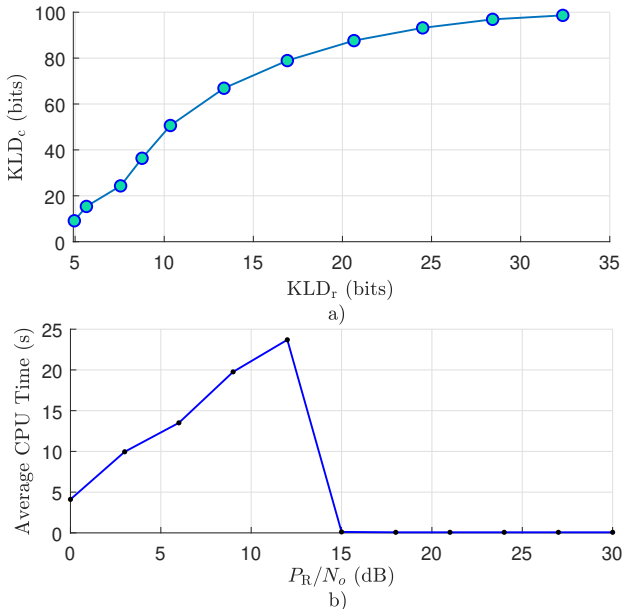


Fig. 9. a) The trade-off performance between the two subsystems KLD_c versus KLD_r . b) The average CPU time (seconds) versus P_R/N_o .

VIII. CONCLUSION

This paper has proposed and validated a novel KLD-based framework for optimising ISAC systems. The two considered

optimisation techniques, namely, KLD-based radar waveform optimisation and KLD-based communication precoding optimisation, demonstrated significant improvements over non-optimised scenarios. Radar waveform KLD-based optimisation yielded substantial enhancements in both target detection and communication performance, as evidenced by the ROC curves and reduced BER across all UEs. Communication KLD-based precoding optimisation, while primarily benefiting the communication subsystem, also showed modest improvements in radar performance, particularly at lower SNRs. Both techniques exhibited robust performance across varying SNR levels, with radar waveform KLD-based optimisation demonstrating stable computational efficiency. Moreover, trade-off analysis revealed that incorporating the communication signal in radar detection significantly enhances the overall ISAC system performance. These findings provide valuable insights for designing and optimising shared deployment ISAC systems, offering a promising approach to balance sensing and communication requirements in future wireless networks. The proposed framework provides the means for a holistic ISAC design, paving the way for more efficient and versatile wireless communications and sensing technologies.

APPENDIX

This appendix provides detailed derivations for the gradients used in our optimisation problem.

A. Gradients for Radar-Waveform Optimisation

The objective function $f(\dot{\mathbf{W}}_r)$ is given in (39), where the $KLD_{r,t}$ is defined in (36). Therefore, to derive $\nabla f(\dot{\mathbf{W}}_r)$, we first compute $\partial KLD_{r,t} / \partial \mathbf{W}_{r,t}$. Using the matrix identity $\frac{\partial \ln(\det(\mathbf{X}))}{\partial \mathbf{X}} = (\mathbf{X}^{-1})^T$, we obtain,

$$\frac{\partial \ln(\det(\mathbf{R}_{2,t}))}{\partial \mathbf{R}_{2,t}} = \mathbf{R}_{2,t}^{-1} \quad (58)$$

For the trace term, applying $\frac{\partial \text{Tr}(\mathbf{X}^{-1}\mathbf{A})}{\partial \mathbf{X}} = -(\mathbf{X}^{-1})^T \mathbf{A}^T (\mathbf{X}^{-1})^T$ yields,

$$\frac{\partial \text{Tr}(\mathbf{R}_{2,t}^{-1}(\sigma_n^2 \mathbf{I}_N))}{\partial \mathbf{R}_{2,t}} = -\sigma_n^2 \mathbf{R}_{2,t}^{-2} \quad (59)$$

Applying the chain rule to (36), and substituting (58) and (59), we get,

$$\frac{\partial KLD_{r,t}}{\partial \mathbf{W}_{r,t}} = \frac{1}{\ln 2} (\mathbf{R}_{2,t}^{-1} - \sigma_n^2 \mathbf{R}_{2,t}^{-2}) \cdot \frac{\partial \mathbf{R}_{2,t}}{\partial \mathbf{W}_{r,t}} \quad (60)$$

where $\frac{\partial \mathbf{R}_{2,t}}{\partial \mathbf{W}_{r,t}} = \frac{d_{r,t}^{\zeta}}{L} \mathbf{H}_t^H \mathbf{H}_t \mathbf{W}_{r,t}$. Substituting this into (60) and simplifying, we obtain,

$$\frac{\partial KLD_{r,t}}{\partial \mathbf{W}_{r,t}} = \frac{d_{r,t}^{\zeta}}{L \ln 2} (\mathbf{H}_t^H \mathbf{R}_{2,t}^{-1} \mathbf{H}_t \mathbf{W}_{r,t} - \sigma_n^2 \mathbf{H}_t^H \mathbf{R}_{2,t}^{-2} \mathbf{H}_t \mathbf{W}_{r,t}) \quad (61)$$

Finally, the gradient of f with respect to $\mathbf{W}_{r,t}$, derived from (39) and (61), is,

$$[\nabla f(\dot{\mathbf{W}}_r)]_{i,l,t} = \frac{2 d_{r,t}^{\zeta}}{TL \ln 2} (\mathbf{H}_t^H (\mathbf{R}_{2,t})^{-1} \mathbf{H}_t \mathbf{W}_{r,t} - \sigma_n^2 (\mathbf{R}_{2,t})^{-2} \mathbf{H}_t \mathbf{W}_{r,t})_i \quad (62)$$

For $\text{KLD}_{c,k}$ gradient calculations, we consider how changes in \mathbf{W}_r affect σ_η^2 , where it is defined as follows,

$$\sigma_\eta^2 = d_{c,k}^\zeta \sigma_h^2 \text{Tr} \left(\frac{1}{L} \sum_{l=1}^L \mathbf{W}_{r,l} \mathbf{W}_{r,l}^H \right) + \sigma_n^2 \quad (63)$$

The derivative of σ_η^2 with respect to $\mathbf{W}_{r,l}$ is,

$$\frac{\partial \sigma_\eta^2}{\partial \mathbf{W}_{r,l}} = \frac{2 d_{c,k}^\zeta \sigma_h^2}{L} \mathbf{W}_{r,l} \quad (64)$$

Computing $\partial \text{KLD}_{c,k} / \partial \sigma_\eta^2$,

$$\frac{\partial \text{KLD}_{c,k}}{\partial \sigma_\eta^2} = -\frac{\lambda d_{c,k}^\zeta p_k (N - K)}{M(M - 1) \sigma_\eta^2 \ln 2} \quad (65)$$

Utilising the chain rule and (64), (65), we obtain,

$$\frac{\partial \text{KLD}_{c,k}}{\partial \mathbf{W}_{r,l}} = -\frac{2\lambda d_{c,k}^\zeta p_k (N - K) \sigma_h^2}{M(M - 1) L \sigma_\eta^2 \ln 2} \mathbf{W}_{r,l} \quad (66)$$

Therefore, the gradient of $\text{KLD}_{c,k}$ with respect to $\dot{\mathbf{W}}_r$ is,

$$[\nabla \text{KLD}_{c,k}]_{i,l,t} = -\frac{2\lambda d_{c,k}^\zeta p_k (N - K) \sigma_h^2}{M(M - 1) L \sigma_\eta^2 \ln 2} [\dot{\mathbf{W}}_r]_{i,l,t} \quad (67)$$

Equations (62) and (67) provide the mathematical foundation for the gradients used in our optimization algorithm.

REFERENCES

- [1] K. Zheng *et al.*, "Reliable and efficient autonomous driving: the need for heterogeneous vehicular networks," *IEEE Commun. Mag.*, vol. 53, no. 12, pp. 72–79, 2015.
- [2] D. C. Nguyen *et al.*, "6G Internet of Things: A Comprehensive Survey," *IEEE Internet Things J.*, vol. 9, no. 1, pp. 359–383, 2022.
- [3] P. Porabage *et al.*, "The Roadmap to 6G Security and Privacy," *IEEE Open J. Commun. Soc.*, vol. 2, pp. 1094–1122, 2021.
- [4] M. Alsabah *et al.*, "6G Wireless Communications Networks: A Comprehensive Survey," *IEEE Access*, vol. 9, pp. 148 191–148 243, 2021.
- [5] ERICSSON, "Joint communication and sensing in 6G networks," *Technical Report*, Oct. 2021. [Online]. Available: <https://tinyurl.com/wt5t7dwd>
- [6] N. Rajatheva *et al.*, "White Paper on Broadband Connectivity in 6G," *arXiv preprint arXiv:2004.14247*, 2020. [Online]. Available: <https://doi.org/10.48550/arXiv.2004.14247>
- [7] M. M. Azari *et al.*, "Evolution of Non-Terrestrial Networks From 5G to 6G: A Survey," *IEEE Commun. Surv. Tutor.*, vol. 24, no. 4, pp. 2633–2672, 2022.
- [8] A. Liu *et al.*, "A Survey on Fundamental Limits of Integrated Sensing and Communication," *IEEE Commun. Surveys Tuts.*, vol. 24, no. 2, pp. 994–1034, 2022.
- [9] F. Liu, C. Masouros, A. Li, and T. Ratnarajah, "Robust MIMO Beamforming for Cellular and Radar Coexistence," *IEEE Wireless Commun. Lett.*, vol. 6, no. 3, pp. 374–377, 2017.
- [10] F. Liu *et al.*, "Toward Dual-functional Radar-Communication Systems: Optimal Waveform Design," *IEEE Trans. Signal Process.*, vol. 66, no. 16, pp. 4264–4279, 2018.
- [11] M. Temiz, E. Alsusa, and M. W. Baidas, "A Dual-Functional Massive MIMO OFDM Communication and Radar Transmitter Architecture," *IEEE Trans. Veh. Technol.*, vol. 69, no. 12, pp. 14 974–14 988, 2020.
- [12] —, "Optimized Precoders for Massive MIMO OFDM Dual Radar-Communication Systems," *IEEE Trans. Commun.*, vol. 69, no. 7, pp. 4781–4794, 2021.
- [13] J. A. Zhang *et al.*, "An Overview of Signal Processing Techniques for Joint Communication and Radar Sensing," *IEEE J. Sel. Topics Signal Process.*, vol. 15, no. 6, pp. 1295–1315, 2021.
- [14] F. Liu *et al.*, "MU-MIMO Communications With MIMO Radar: From Co-Existence to Joint Transmission," *IEEE Trans. Wireless Commun.*, vol. 17, no. 4, pp. 2755–2770, 2018.
- [15] C. Xu, B. Clerckx, and J. Zhang, "Multi-Antenna Joint Radar and Communications: Precoder Optimization and Weighted Sum-Rate vs Probing Power Tradeoff," *IEEE Access*, vol. 8, pp. 173 974–173 982, 2020.
- [16] N. Fatema *et al.*, "Massive MIMO Linear Precoding: A Survey," *IEEE Syst. J.*, vol. 12, pp. 3920–3931, 2018.
- [17] C. Ouyang, Y. Liu, and H. Yang, "Performance of Downlink and Uplink Integrated Sensing and Communications (ISAC) Systems," *IEEE Wireless Communications Letters*, vol. 11, no. 9, pp. 1850–1854, 2022.
- [18] B. Tang, M. M. Naghsh, and J. Tang, "Relative Entropy-Based Waveform Design for MIMO Radar Detection in the Presence of Clutter and Interference," *IEEE Trans. Signal Process.*, vol. 63, no. 14, pp. 3783–3796, 2015.
- [19] J. Tang, N. Li, Y. Wu, and Y. Peng, "On Detection Performance of MIMO Radar: A Relative Entropy-Based Study," *IEEE Signal Process. Lett.*, vol. 16, no. 3, pp. 184–187, 2009.
- [20] Y. Kloob, M. Al-Jarrah, E. Alsusa, and C. Masouros, "Trade-Off Performance Analysis of Radcom Using the Relative Entropy," in *Proc. IEEE Symp. Comput. Commun. (ISCC) 2024*, pp. 1–6, 2024.
- [21] M. Al-Jarrah, E. Alsusa, and C. Masouros, "A Unified Performance Framework for Integrated Sensing-Communications based on KL-Divergence," *IEEE Trans. Wireless Commun.*, pp. 1–1, 2023.
- [22] —, "Kullback-Leibler Divergence Analysis for Integrated Radar and Communications (RadCom)," in *2023 IEEE Wireless Commun. Netw. Conf. (WCNC)*, 2023, pp. 1–6.
- [23] Y. Kloob, M. Al-Jarrah, E. Alsusa, and C. Masouros, "Novel KLD-based Resource Allocation for Integrated Sensing and Communication," *IEEE Trans. Signal Process.*, vol. 72, pp. 2292–2307, 2024.
- [24] Z. Fei *et al.*, "Revealing the trade-Off in ISAC systems: The KL divergence perspective," *IEEE Wireless Commun. Lett.*, pp. 1–1, 2024.
- [25] F. Liu *et al.*, "Cramér-Rao Bound Optimization for Joint Radar-Communication Beamforming," *IEEE Trans. Signal Process.*, vol. 70, pp. 240–253, 2022.
- [26] X. Wang, Z. Fei, J. A. Zhang, and J. Xu, "Partially-Connected Hybrid Beamforming Design for Integrated Sensing and Communication Systems," *IEEE Trans. Commun.*, vol. 70, no. 10, pp. 6648–6660, 2022.
- [27] Z. Liao and F. Liu, "Symbol-Level Precoding for Integrated Sensing and Communications: A Faster-Than-Nyquist Approach," *IEEE Communications Letters*, vol. 27, no. 12, pp. 3210–3214, 2023.
- [28] A. Hassaniien, M. G. Amin, Y. D. Zhang, and F. Ahmad, "Signaling strategies for dual-function radar communications: an overview," *IEEE Aerosp. Electron. Syst. Mag.*, vol. 31, no. 10, pp. 36–45, 2016.
- [29] P. Kumari, J. Choi, N. González-Prelcic, and R. W. Heath, "IEEE 802.11ad-Based Radar: An Approach to Joint Vehicular Communication-Radar System," *IEEE Trans. Veh. Technol.*, vol. 67, no. 4, pp. 3012–3027, 2018.
- [30] H. Xu, R. S. Blum, J. Wang, and J. Yuan, "Collocated MIMO radar waveform design for transmit beampattern formation," *IEEE Trans. Aerosp. Electron. Syst.*, vol. 51, no. 2, pp. 1558–1568, 2015.
- [31] A. Hassaniien and S. A. Vorobyov, "Phased-MIMO Radar: A Tradeoff Between Phased-Array and MIMO Radars," *IEEE Trans. Signal Process.*, vol. 58, no. 6, pp. 3137–3151, 2010.
- [32] H. Zhang, B. Zong, and J. Xie, "Power and Bandwidth Allocation for Multi-Target Tracking in Collocated MIMO Radar," *IEEE Trans. Veh. Technol.*, vol. 69, no. 9, pp. 9795–9806, 2020.
- [33] H. Zhang *et al.*, "Antenna Selection for Target Tracking in Collocated MIMO Radar," *IEEE Trans. Aerosp. Electron. Syst.*, vol. 57, no. 1, pp. 423–436, 2021.
- [34] W. Yi, T. Zhou, Y. Ai, and R. S. Blum, "Suboptimal Low Complexity Joint Multi-Target Detection and Localization for Non-Coherent MIMO Radar With Widely Separated Antennas," *IEEE Trans. Signal Process.*, vol. 68, pp. 901–916, 2020.
- [35] E. Fishler *et al.*, "Spatial Diversity in Radars—Models and Detection Performance," *IEEE Trans. Signal Process.*, vol. 54, no. 3, pp. 823–838, 2006.
- [36] J. Nocedal and S. J. Wright, *Numerical Optimization*, 2nd ed. Springer, 2006.
- [37] D. P. Bertsekas, *Nonlinear Programming*, 2nd ed. Athena Scientific, 1999.
- [38] L. Armijo, "Minimization of functions having Lipschitz continuous first partial derivatives," *Pacific Journal of Mathematics*, vol. 16, no. 1, pp. 1–3, 1966.
- [39] A. Forsgren, P. E. Gill, and M. H. Wright, "Interior Methods for Nonlinear Optimization," *SIAM Review*, vol. 44, no. 4, pp. 525–597, 2002. [Online]. Available: <https://doi.org/10.1137/S0036144502414942>